Supplementary Information

Metal-support interactions alter the active species on IrO$_x$ for electrocatalytic water oxidation

*Ge-Yang Xu,[a] Mu-Fei Yue,[a] Zheng-Xin Qian,[a] Zi-Yu Du,[a] Xiao-Qun Xie,[a] Wei-Ping Chen,[a] Yue-Jiao Zhang,[*a] and Jian-Feng Li[*abc]*

a. College of Energy, State Key Laboratory of Physical Chemistry of Solid Surfaces, iChEM, College of Chemistry and Chemical Engineering, College of Materials, Xiamen University, Xiamen 361005, China. Email: zhangyuejiao@xmu.edu.cn, li@xmu.edu.cn

b. Innovation Laboratory for Sciences and Technologies of Energy Materials of Fujian Province (IKKEM), Xiamen 361005, China

c. College of Optical and Electronic Technology, China Jiliang Unversity, Hangzhou 310018, China

Detailed calculation of mass activity and Turnover frequency (TOF) values

The mass activities of OER catalysts were calculated based on the linear sweeping voltammograms.

$$mass\ activity = j/m \text{ (S1)}$$

j (mA/cm^2) is the measured current density at an overpotential of 300 mV. **m** (mg/cm^2) is the electrocatalyst loading on the working electrode.

$$TOF = (j \times A)/(4 \times F \times n) \text{ (S2)}$$

j (mA/cm^2) is the measured current density at an overpotential of 300 mV. A is the geometric area of the working electrode (0.196 cm^2). F is the faraday constant of 96485 C/mol. n is the number of moles of Ir atoms on the working electrode. **n=m/M**, **m** (mg/cm^2) is the electrocatalyst loading on the working electrode. M (g/mol) is the molecular weight of Ir.

Preparation of Au@MnO$_2$-IrO$_x$-a nanoparticles

First, ~16 nm Au nanoparticles were prepared as the inner cores. 2.424 mL 1% HAuCl$_4$·4H$_2$O solution was added to 200 mL de-ionized (DI) water. The solution was heated to a boil, and then 4 mL 1% sodium citrate solution was quickly injected under vigorous stirring. The color of the system would chang from faint yellow to wine red in a few minutes, which indicated ~16 nm Au NPs colloid was successfully synthesized. The heat and stirring should be kept in half an hour at least to assure the completeness of the reaction. Then, the system was cooled to ambient temperature naturally.

Second, Au@MnO$_2$ (~8 nm) NPs were prepared by the following procedure: 10 mL ~16 nm Au NPs colloid was cooled to 4°C in the ice bath, followed by injection of 170 μL 0.1 M KOH solution and 0.5 mL 10 mM KMnO$_4$ solution under stirring. 2.5 mL 10 mM K$_2$C$_2$O$_4$ solution was dropped into the system gradually. The reaction was kept stirring in the ice bath for one hour and then transferred to 60 °C water bath for 3 hours. At last, the colloid through naturally cooling was centrifuged and washed twice.

Third, Au@MnO$_2$-IrO$_x$ (a) NPs were fabricated referring to the Experiment section.

Preparation of Au@MnO$_2$-IrO$_x$-b nanoparticles

Au@MnO$_2$ colloid was dispersed by 10 mL DI water, followed by the addition of 1 mL 2.5 mM IrCl$_3$ solution. The system was kept stirring for 5 h at the ambient temperature. And then, 200 μL 10 mM NaBH$_4$ solution was injected slowly. At last, the colloid was centrifuged and washed twice.

The mass formulas for calculation of isotopic shifts

As the peak at 1062 cm^{-1} was assigned to *O-O$^-$ species, the ratio (γ) of the Raman frequency for *O-O$^-$ downward shift in the H$_2$^{18}O experiment can be approximately analyzed by following mass formula:

$$\gamma = \frac{v\left(^{18}O^{18}O\right)}{v\left(^{16}O^{16}O\right)} = \frac{\sqrt{m\left(^{18}O\right) + m\left(^{18}O\right)}}{\sqrt{m\left(^{18}O\right) \times m\left(^{18}O\right)}} \Bigg/ \frac{\sqrt{m\left(^{16}O\right) + m\left(^{16}O\right)}}{\sqrt{m\left(^{16}O\right) \times m\left(^{16}O\right)}} = 94.28\%$$

$$\gamma = \frac{v\left(^{16}O^{18}O\right)}{v\left(^{16}O^{16}O\right)} = \frac{\sqrt{m\left(^{16}O\right) + m\left(^{18}O\right)}}{\sqrt{m\left(^{16}O\right) \times m\left(^{18}O\right)}} \Bigg/ \frac{\sqrt{m\left(^{16}O\right) + m\left(^{16}O\right)}}{\sqrt{m\left(^{16}O\right) \times m\left(^{16}O\right)}} = 97.12\%$$

The 1062 cm^{-1} peak on Au@MnO$_2$-IrO$_x$ shifted to about 1004 cm^{-1} in the H$_2$^{18}O experiments. The experimental shift ratio was 94.54%, consistent with the theoretical shift ratio of ^{18}O-^{18}O.

DFT Calculation methods

Spin polarization calculations were carried out by using the Vienna ab initio simulation package (VASP).[1] The valence electrons were described by plane wave basis set with a cutoff energy of 450 eV, and the core electrons were replaced by the projector augmented wave pseudopotentials.

Brillouin zone integrations were performed using Monkhorst-Pack gird of 7 * 7 * 1 for the slab calculations. For all kinds of Gibbs free energy calculations, the k-points mesh was set to 9 * 79* 1, because increasing the k-points mesh to higher values did not produce observable energy differences, suggesting that 9 * 9 * 1 mesh was sufficient to achieve high calculation accuracy.

Exchange and correlation were treated within Perdew-Burke-Ernzerhof (PBE)

generalized gradient approximation (GGA).[2] The Gaussian searing method was employed to determine the electron occupancies, with a smearing parameter σ of 0.2 eV.

For the IrO_2 clusters, we constructed the structure using the cell parameters obtained from IrO_2. IrO_2 cluster was put on a monolayer of δ-MnO_2 slab.
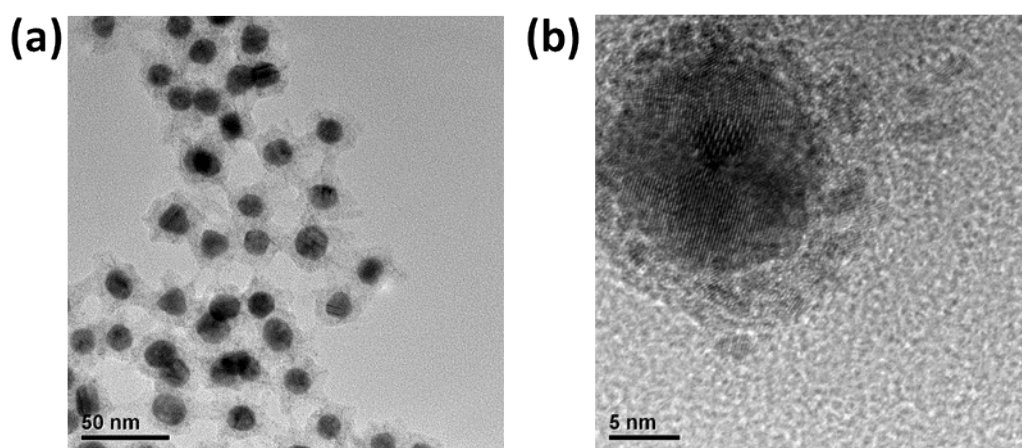

Figure S1. HRTEM images of Au@MnO_2-IrO_x-a NPs
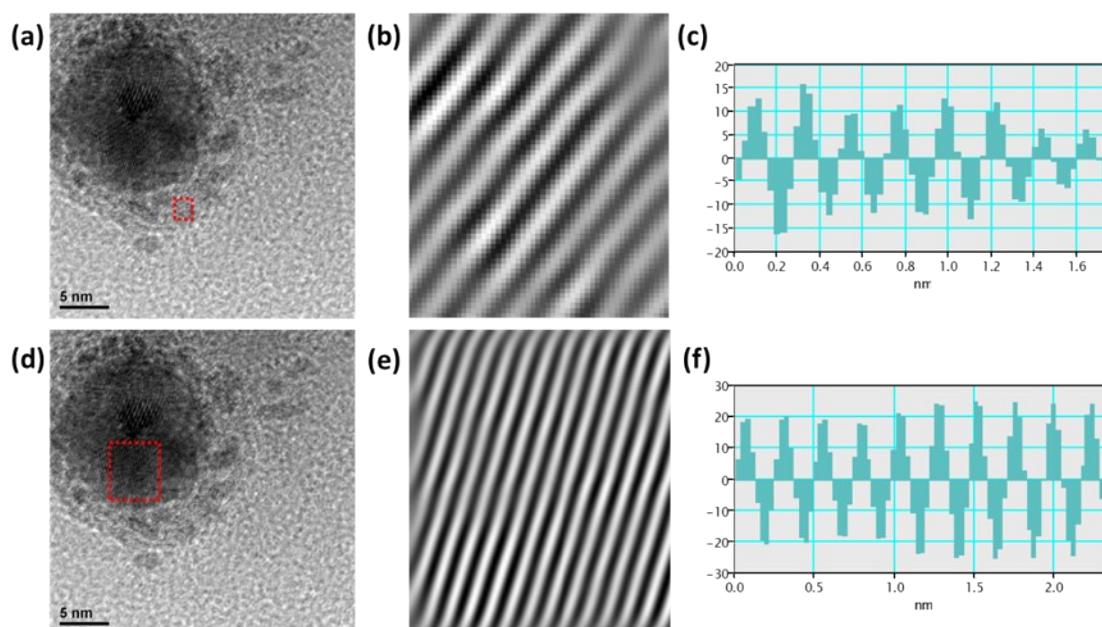
Figure S2. (a) HRTEM image of the Au@MnO_2-IrO_x-a NPs. (b) Lattice stripes processed from red region in (a). (c) Crystal plane spacing processed from (b). (d) HRTEM image of the Au@MnO_2-IrO_x-a NPs. (e) Lattice stripes processed from red region in (d). Crystal plane spacing processed from (e).

Table S1. ICP-OES test results of Au@MnO$_2$-IrO$_x$ NPs

Element	Au	Mn	Ir
Mass proportion (%)	98.93	0.70	0.37

Table S2. Comparison of OER activity of electrocatalysts with other reported catalysts

Catalysts	Mass activity(A/g$_{metal}$)	Overpotential at 10 mA/cm^2(mV)	Solution
Ir$_1$-Ni(OH)$_2$[3]	1867(@300 mV)	260	1 M KOH
np-Ir/NiFeO[4]	39300(@250 mV)	197	1 M KOH
3D Ir[5]	~1910(@250 mV)	240	1 M KOH
Ir-PdCu[6]	1010(@300 mV)	284	0.1 M KOH
Ir-V$_2$O$_5$[7]	207(@300 mV)	283	1 M KOH
IrNi$_2$[8]	130(@250 mV)	-	0.1 M KOH
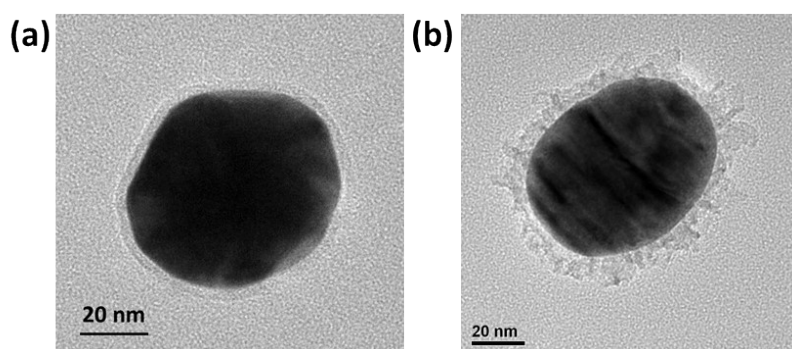
Figure S3. TEM image of Au@MnO$_2$ NPs with shells about 3nm (a) and 8nm (b).
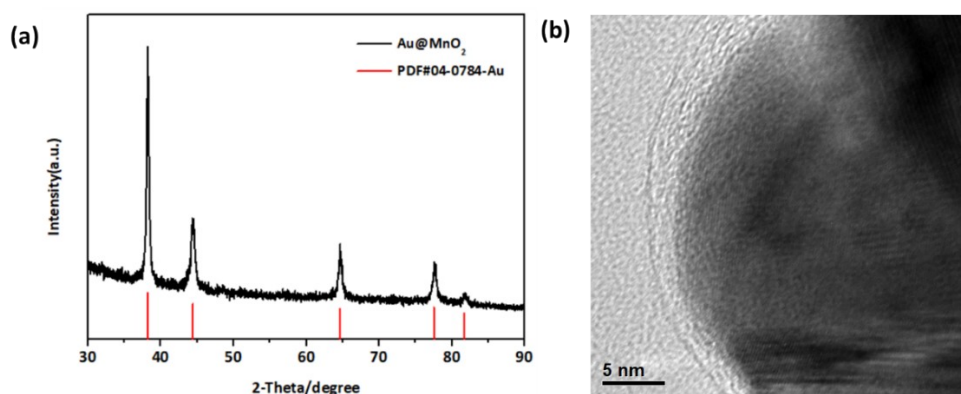
Figure S4. (a) XRD pattern of Au@MnO$_2$ NPs. (b) HRTEM image of Au@MnO$_2$ NPs.

(a)

Au@8 nmMnO₂

δ-MnO₂ powder

Raman shift(cm⁻¹)

(b)

Au@MnO₂

Mn 2p₃/₂
642.0 eV

Mn 2p₅/₂
653.8 eV

Intentity(a.u.)

Binding Energy(eV)
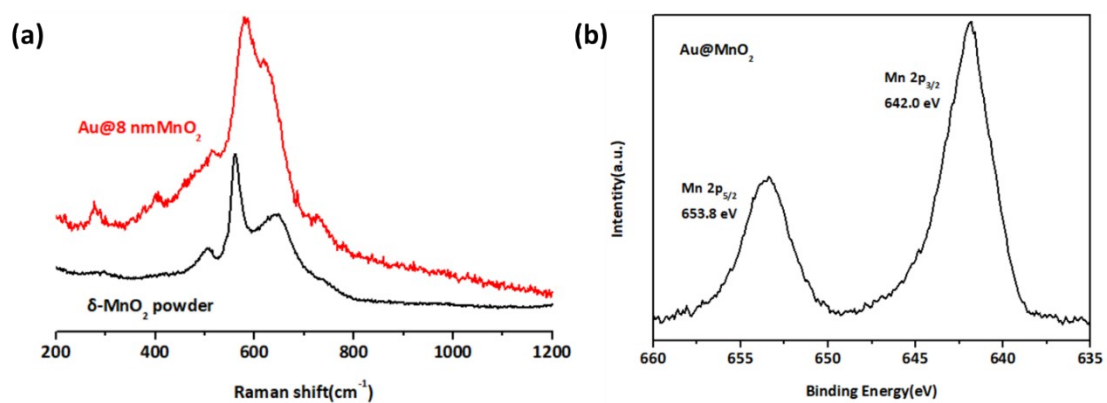
Figure S5. (a) Raman spectra of Au@8 nm MnO_2 NPs and δ-MnO_2 powder. (b)XPS spectra of Au@MnO_2 NPs.

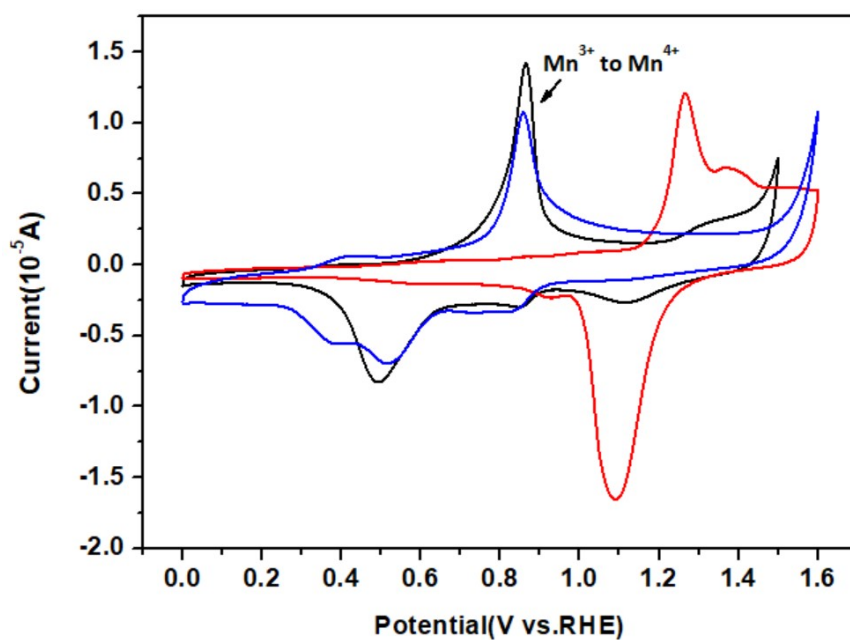Mn^{3+} to Mn^{4+}

Current(10⁻⁵ A)

Potential(V vs.RHE)

Figure S6. Cyclic voltammograms (CV) of samples on glass carbon (GC) electrodes with a scan rate of 50 mV/s. black line: Au@MnO_2-IrO_x NPs, blue line: Au@MnO_2 NPs and red line: Au NPs.
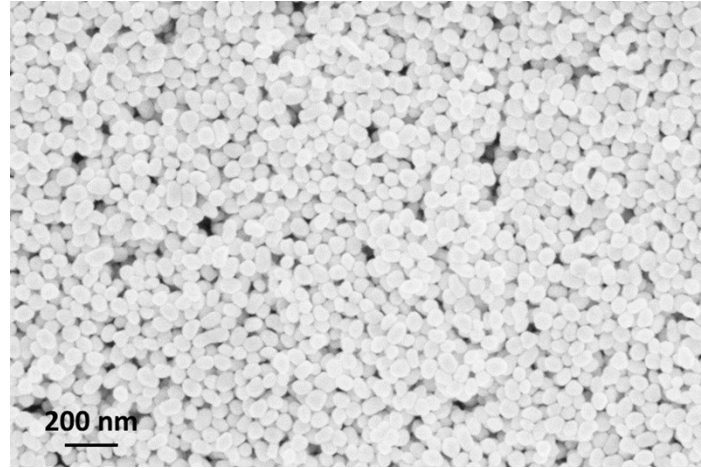
Figure S7. SEM image of Au@MnO$_2$-IrO$_x$ NPs.
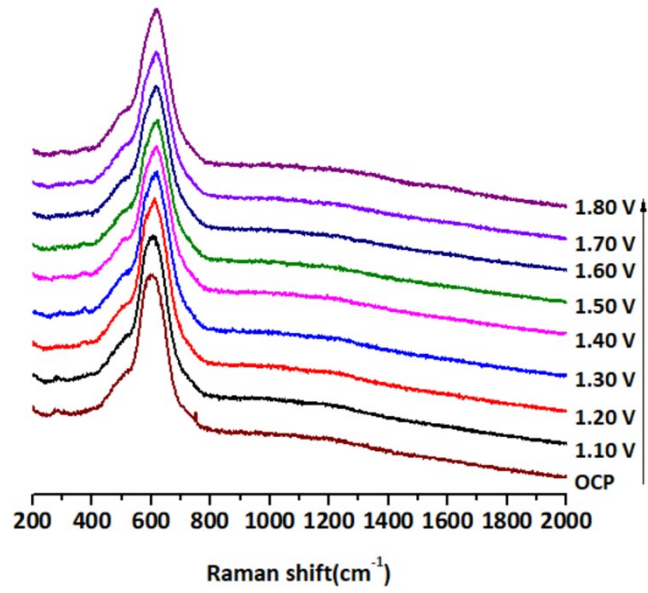
Figure S8. In situ electrochemical SERS of Au@MnO$_2$ NPs.
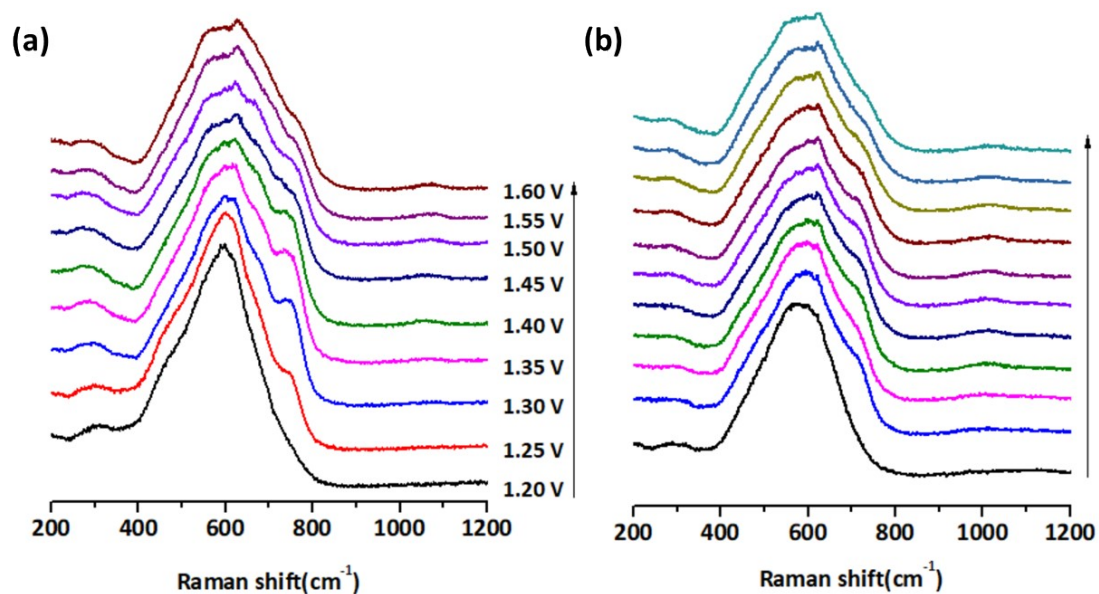
Figure S9. Isotopic Raman experiments of Au@MnO$_2$-IrO$_x$ NPs. (a) D$_2$O experiment. (b) H$_2$^{18}O experiment.
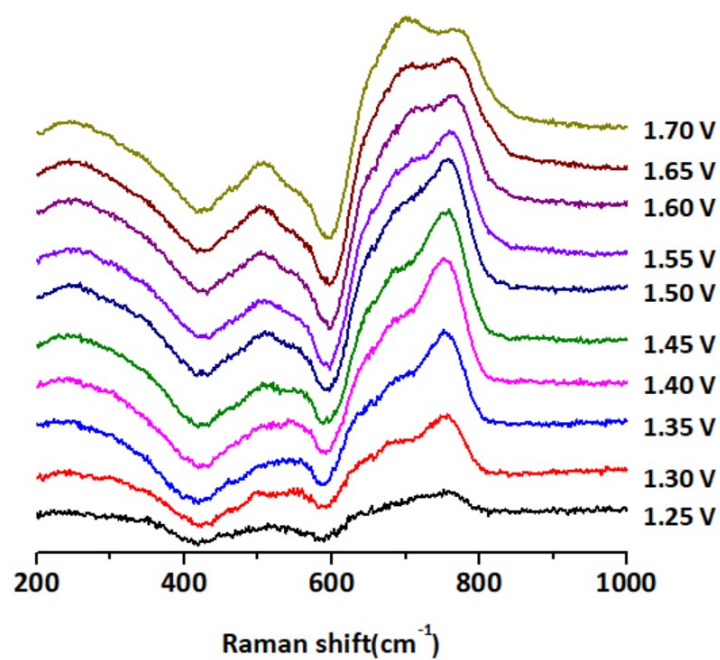

Figure S10. In situ electrochemical SERS of Au@MnO$_2$-IrO$_x$ NPs. The spectra with all the potentials were obtained by subtracting the spectrum at 1.20 V.
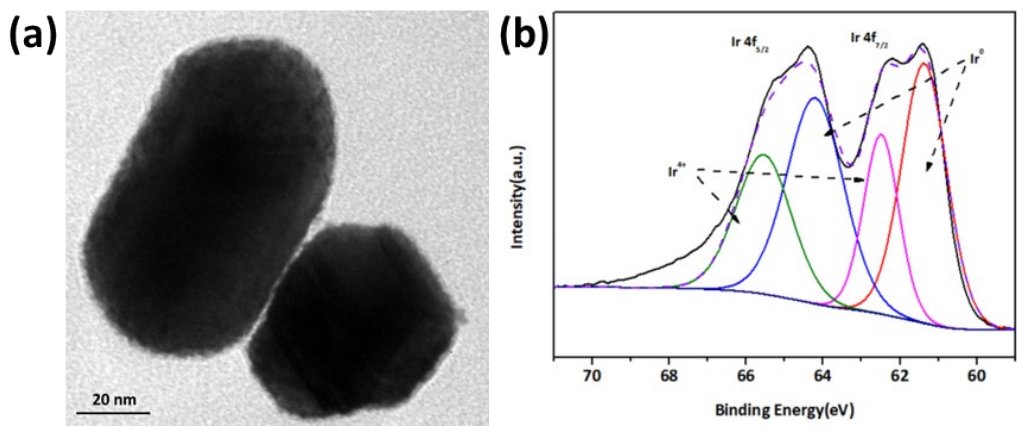
Figure S11. (a) TEM image of Au@Ir NPs. (b) XPS spectra of Au@Ir NPs. These results indicate that Ir^0 and Ir^{4+} coexist in the shell, and IrO_2 species distribute outside the metal Ir.
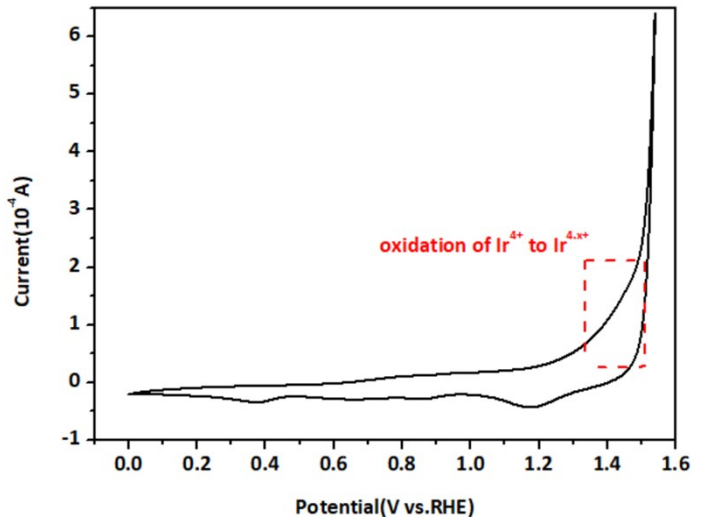

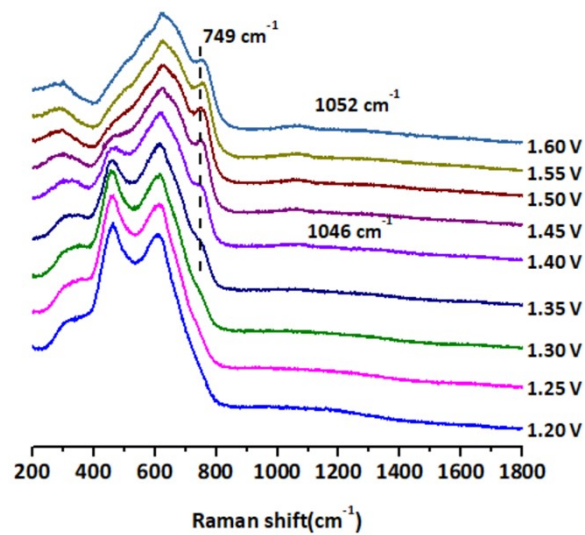**Figure S12.** CV of Au@Ir NPs on glass carbon (GC) electrodes with a scan rate of 50 mV/s.

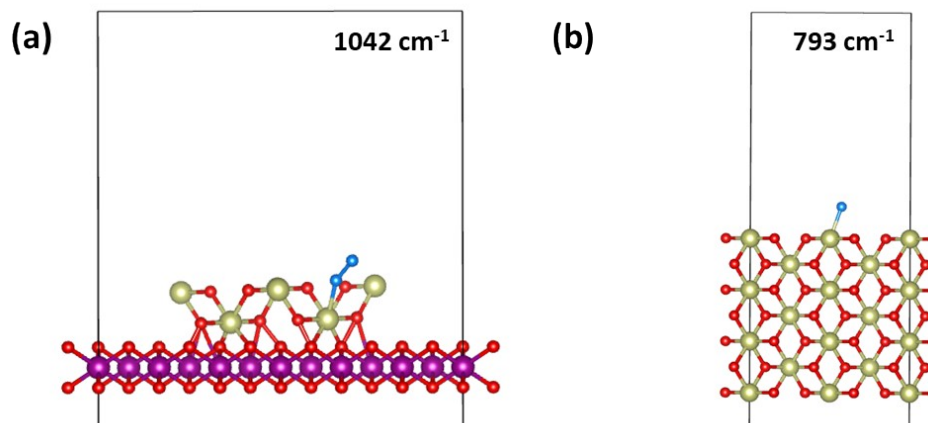**Figure S13.** In situ electrochemical SERS of Au@MnO$_2$-IrO$_x$-b NPs.

Figure S14. Theoretical Raman shifts of *O-O- on MnO$_2$-IrO$_2$(a) and *O on IrO$_2$ (b) species and their schematic models for DFT calculations.

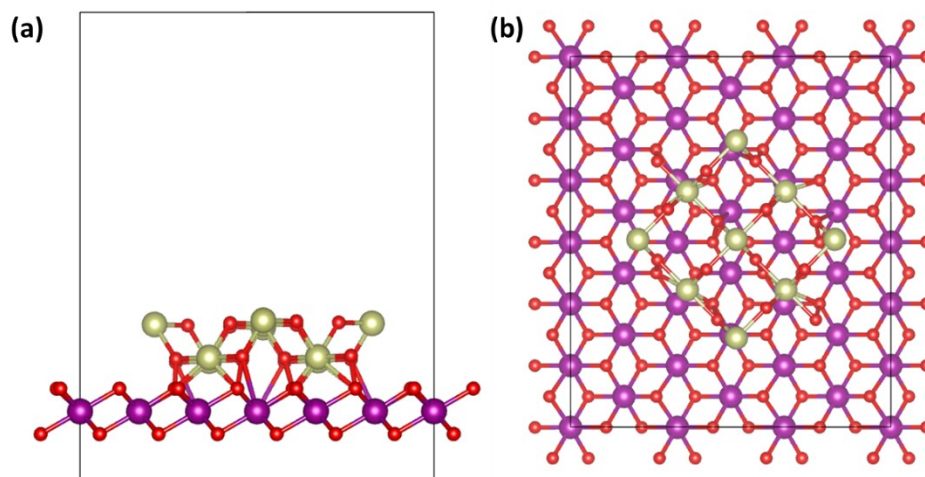**Figure S15.** Schematic models of MnO_2-IrO_2 for DFT calculations, side view (a) and top view (b).
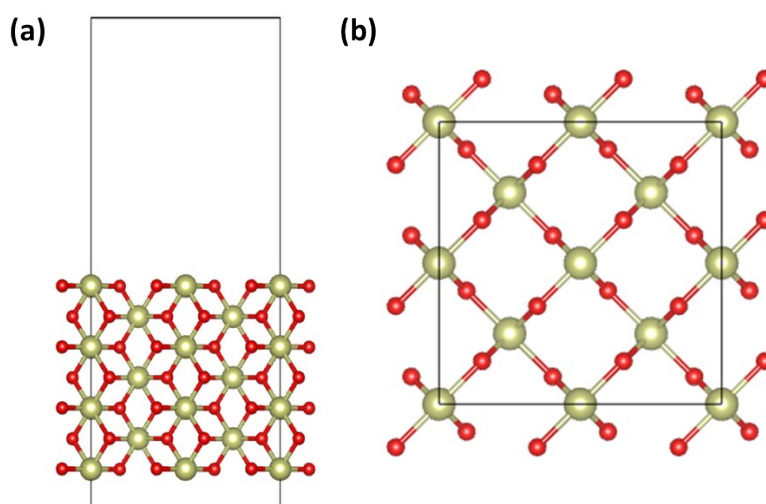

Figure S16. Schematic models of IrO_2 for DFT calculations, side view (a) and top view (b).

1.   G. Kresse and J. Furthmüller, *Phys. Rev. B*, 1996, **54**, 11169-11186.
2.   J. P. Perdew, K. Burke and M. Ernzerhof, *Phys. Rev. Lett.*, 1996, **77**, 3865-3868.
3.   Q. He, S. Qiao, Q. Zhou, Y. Zhou, H. Shou, P. Zhang, W. Xu, D. Liu, S. Chen, X. Wu and L. Song, *Nano. Lett.*, 2022, **22**, 3832-3839.
4.   K. Jiang, M. Luo, M. Peng, Y. Yu, Y. R. Lu, T. S. Chan, P. Liu, F. M. F. de Groot and Y. Tan, *Nat. Commun.*, 2020, **11**, 2701.
5.   Y. Pi, N. Zhang, S. Guo, J. Guo and X. Huang, *Nano. Lett.*, 2016, **16**, 4424-4430.
6.   Y. Qin, Z. Wang, W. Yu, Y. Sun, D. Wang, J. Lai, S. Guo and L. Wang, *Nano. Lett.*, 2021, **21**, 5774-5781.

7.   X. Zheng, M. Qin, S. Ma, Y. Chen, H. Ning, R. Yang, S. Mao and Y. Wang, *Adv. Sci.,* 2022, **9**, e2104636.
8.   Y. Pi, Q. Shao, X. Zhu and X. Huang, *ACS Nano*, 2018, **12**, 7371-7379.